Self-compression of high energy ultrashort laser pulses

Qiandong Ran,[1] Hao Li,[1,] Wonkeun Chang,[2] and Qi Jie Wang[2]*

[1]*Singapore Institute of Manufacturing Technology (SIMTech), Agency for Science, Technology and Research (A*STAR), 2 Fusionopolis Way, Innovis, #08-04, Singapore 138634, Republic of Singapore*
[2]*School of Electrical and Electronic Engineering, Nanyang Technological University, 50 Nanyang Ave, Singapore 639798, Republic of Singapore*
**hli@simtech.a-star.edu.sg*

Keywords: ultrafast laser, pulse compression, ultrashort pulse generation, high power laser

Abstract: Nonlinear pulse compression techniques have been applied widely in the pursuit of ultra-intense laser pulse with extreme high pulse energy (~mJ) and extreme short pulse duration (~sub-10 fs). Although post compression techniques using dispersive gratings or chirped mirrors have achieved 1 TW few-cycle pulses, further increasing of the pulse intensity is limited by the damage threshold of dispersive optics, especially when self-focusing and ionization in the propagation medium are considered. To overcome such limitations, ultrashort pulses self-compression techniques without vulnerable dispersive optics have been explored in the past two decades. In this paper, latest advances in these techniques will be reviewed with a discussion on the progress of various experimental approaches as well as their potential applications and roles in generating extremely intense optical fields for strong-field physics research.

1. Introduction

Ultrashort pulse laser technology has opened the door to explore the ultrafast nonlinear phenomena, including high harmonic generation [1-4], laser particle acceleration [5, 6] and ultrafast spectroscopy [7]. These all benefit from the ultrashort pulse duration and high laser intensity. For an optical Gaussian pulse in a Gaussian beam, the peak intensity at the focus of the beam is

$$I = \frac{1.88\varepsilon}{\pi w^2 \tau} \quad (1)$$

where ε is the pulse energy; w is the 1/e^2 radius of the beam; τ is the full width at half maximum (FWHM) pulse duration. From Equation (1), we can see that the peak intensity of the laser can be increased through either enhancing the total pulse energy or confining all the laser energy into an as small as possible spatial-temporal domain, through both extremely tight focusing and temporally pulse duration compression. All these approaches have been well studied and successfully demonstrated in lower power regime in the experiments such as high efficiency power amplification, diffraction limited focusing or Fourier transform limited laser pulse compression. However, with the breakthrough of the laser technology in the past few decades, TW and even PW laser systems have been developed. For such high-power laser systems, confining the pulse energy (mJ to J) in spatial or temporal domain becomes more challenging. On the one hand, the continuously increased laser intensity has reached the regime of the nonlinear optics. The optical nonlinearity induced can be quantified by B-integral $B = \frac{2\pi}{\lambda}\int n_2 I(z) dz$ where λ is the laser wavelength, n_2 is the nonlinear index of the medium, and $I(z)$ is the laser intensity along the beam axis. With a very high laser intensity $I(z)$, all materials including the air or noble gases show strong optical nonlinearity and lead to strong Kerr lens effect, ionization or filamentation. These nonlinear effects severely degrade the laser beam quality and even destroy it completely. On the other hand, these high-power laser systems can also modify the material itself through photoionization or photo-chemical reaction [8, 9]. Furthermore, the strong fields generated by these laser systems can accelerate some small particles such as electrons, ions, protons to extremely high speed that comparable with light, which leads to the relativistic and nonlinear quantum electrodynamics effects [10-12]. All constraints discussed above make the spatial focusing and temporal compression of laser pulses at high-power level much more complicated as well as much more difficult compared with their implementation at low-power level. However, big challenges often come with high impacts. The compression of high-power optical pulses in spatial and temporal domains has found many exciting applications in strong field laser physics and fundamental quantum systems [13, 14]. Spatial focusing of high-power laser has been well studied and reviewed in some publications such as filamentation in transparent media [15]. In this paper, we will focus on the temporal compression techniques of high-power optical pulses.

To generate ultrashort laser pulses temporally, two requirements are needed: firstly, the spectrum should have enough broad spectral bandwidth to support the targeted ultrashort laser pulse; secondly all spectral components should have synchronized relative phase relationship and a linear or flat phase profile is preferred [16]. Most of the pulse lasers have limited spectrum due to the narrow bandwidths of the gain medium or pump source. Therefore, the most common temporal pulse compression technique is called post compression which is reviewed in a recent paper by Nagy et. al. [17]. Post compression technique normally contains two steps: (1) the spectrum is broadened first in a nonlinear medium; (2) the spectral phase is then compensated by the dispersive optics to obtain the near Fourier transform limited pulse duration. The spectrum broadening step can be achieved in many ways such as free propagation in bulk materials [18], multiple-plate continuum generation [19], or propagation in gas filled multi-pass cells [20] or hollow core fibers (HCF) [21]. However, there are two limitations for post compression techniques. Firstly, the occurrence of self-focusing and ionization in the nonlinear medium degrades the spectral broadening and spatial profiles when the laser intensity is high. Therefore, ionization normally needs to be avoided in the post compression techniques which limit the laser power scaling. Secondly, the phase compensation after the spectral broadening always needs chirped mirrors or gratings which often have limited damage thresholds and bandwidths. This forms a bottleneck for power scaling and further pulse shortening of post compression techniques. To avoid the ionization in air and hot spots in optical elements, researchers can increase the beam size to maintain the laser intensity at a relatively low level over the whole optical path. However, larger crystals and mirrors with high homogeneity and identical surface quality are needed which are quite challenging to synthesize and fabricate. The thermal control to avoid localized hot spots or phase mismatch also becomes very difficult when the size of optical elements increase. Furthermore, the critical power for self-focusing is determined by the pulse peak power not peak intensity [22]. The laser beam with peak power above critical power threshold will undergo self-focusing and lead to ionization eventually. Hence, researchers have tried to exploit the possibility to utilize, instead of avoid or suppress, the ionization for pulse compression [23]. The related theoretical work was done by Tempea and Brabec [24]. To overcome limitations of the dispersive optics in post compression techniques, pulse compression techniques without any chirped mirrors or gratings for phase compensation are explored. These are the pulse compression techniques reviewed in this paper: laser pulse self-compression techniques. As there are no post dispersion compensation optics used, laser pulse self-compression techniques are not hindered by the dispersive optics damage threshold and more suitable for the sustainable power scale-up, especially considering the current fast pace of high-power laser technology development.

In 2000, self-compression of high-intensity femtosecond pulses was first reported in a number of atomic and molecular gases and solid bulk material by Koprinkov et al. [25]. This self-compression represents a new compression method scalable for high energy femtosecond pulses, which does not require subsequent phase compensation stage. They explained this phenomenon with higher order nonlinearity induced by the high laser intensity. In 2004, Wagner et al. demonstrated a self-compression from 30 to 13 fs by propagating pulses inside a hollow core waveguide filled with low-pressure argon gas, without the use of any external dispersion compensation [26]. They claimed that the self-compression is due to a combination of ionization-induced spectral broadening, plasma-induced refraction, and guiding in the hollow core waveguide. On the other hand, the self-compression of laser pulses in filamentation is also under intensive study [27-31]. After the invention of Hollow Core Photonic Crystal Fibre (HC-PCF), soliton self-compression can be achieved in these fibers. Without the bandwidth limitations of phase compensation optics, self-compression techniques have a great potential to achieve the shortest optical pulses down to the sub-cycle regime with multi-octave-spanning spectra. Travers et al. observed self-compression to sub-cycle pulses in conventional large-core hollow capillary fibres [32]. They showed that the further scaling of soliton effects by several orders of magnitude to the multi-mJ energy and terawatt peak power level is possible. Here, this paper will give a review of the works on self-compression of high energy pulses. They are organized by self-compression propagation geometries. Self-compression during free propagation will be first discussed followed by self-compression in waveguides. To clearly understand the mechanisms behind these self-compression methods, we classify them into three categories: ionization-induced self-compression, self-compression by filamentation, and self-compression by solitons. Then their key figures-of-merits (compressed pulse duration, pulse energy, peak power, and average power) are compared. The conclusion and outlook are presented in the last section.

2. Self-compression during free propagation

2.1 Free propagation in solids

In a Kerr medium with a positive nonlinear refractive index, a laser beam self-focuses if the power P is greater than the critical power of self-focusing P_{cr}. This critical power is defined as [22]

$$P_{cr} = \frac{\lambda^2}{2\pi n_0 n_2} \quad (2)$$

Here, λ is the laser wavelength, n_0 and n_2 are the linear and nonlinear parts of the medium's refractive index, respectively. There are two methods in increasing the critical power according to Equation (2): increasing the wavelength or decreasing nonlinear refractive index. For free propagation in solids, increasing the wavelength can be applied because the nonlinear refractive index for solids is large. This is also why most of self-compression works reported in solids are achieved in the mid-infrared range. The self-trapping over distances larger than the Rayleigh length happens as a counterbalance of the self-focusing due to the Kerr effect and the defocusing effect due to the formation of a low-density plasma. Henz et al. predicted that a significant pulse shortening with a compression factor of 5.5 can be achieved in multiphoton-ionized dispersive dielectric solids [33]. The effects of self-steepening and space-time focusing on the pulse shortening are discussed in the work by Ward et al. [34]. Later in 2006, a self-compression from 50 to 20 fs was achieved in BK7 glass with a compression factor of about 2.5 [35]. They claimed that the self-focusing plays a significant role for the self-compression phenomenon although the effect of the higher-order nonlinearity induced by the multiphoton ionization (MPI) and higher-order dispersion is non-negligible. The power scaling for self-compression in solids faces two challenges. First, the damage thresholds of bulk optical materials are usually low (10^{11} W/cm^2 for quartz [36]; 10^{13} W/cm^2 for fused silica [37]). Second, the critical power of self-focusing is relatively low (~MW) in solids because they have large nonlinear refractive indices. Propagation of a beam carrying pulses with high P/P_{cr} ratios over an extended distance results in a rapid beam breakup into multiple filaments and an overall loss of coherence. This limits the energy of the self-compressed pulses in the femtosecond range to a few microjoules for solid media [38]. Therefore, the thickness of solid slabs used in self-compression of pulses with peak power much larger than the critical power must be small. For example, Shumakova et al. achieved multi-millijoule few-cycle mid-infrared pulse through self-compression in a 2 mm yttrium aluminium garnet (YAG) crystal [39] (Figure 1). The power achieved in this work surpassed the critical power of self-focusing by multiple orders of magnitude.

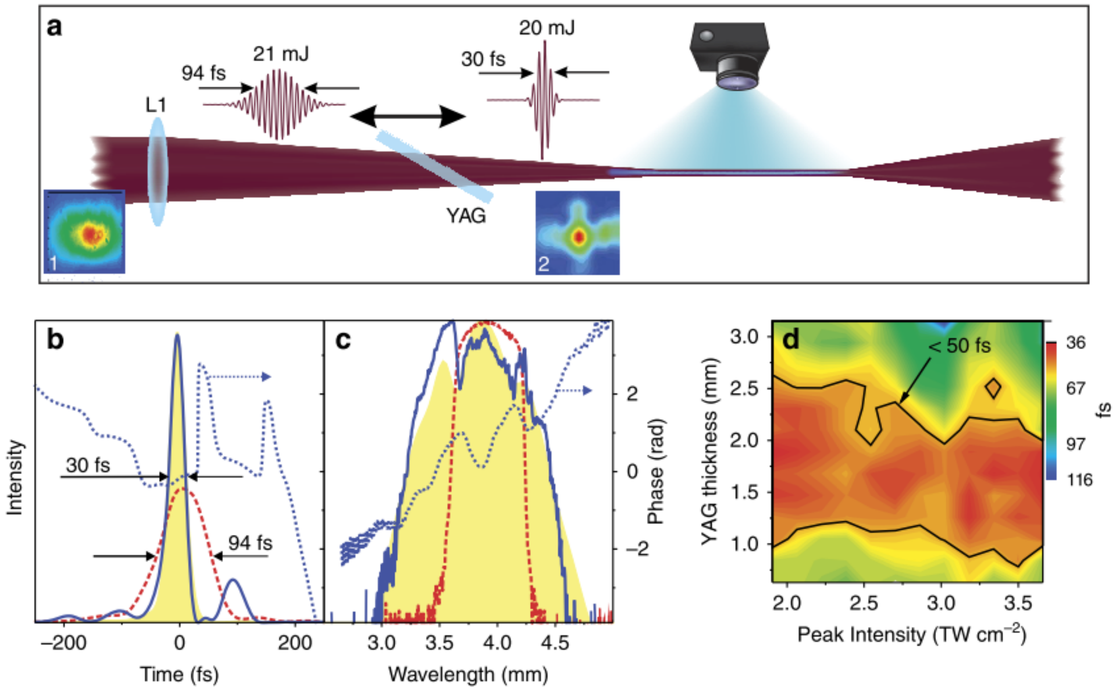

Figure 1. Setup for self-compression in YAG and characterization of compressed pulses [39].

2.2 Free propagation in gas

Compared to solids, the critical power for self-focusing in gas is much higher because the nonlinear refractive index of gas is lower than that of solids by many orders of magnitude. Therefore, higher powers can be applied in the self-compression in gases. In 2000, Koprinkov et al. observed self-compression of high-intensity femtosecond pulses in a number of atomic and molecular gases (Ar, Kr and CH_4) [25]. In another report, stable and uniform self-compression of the laser pulse was achieved by propagating tightly focused mJ femtosecond laser pulses through a gas jet, self-compressing the pulse down to 16 fs from an original 36 fs with low loss [40].

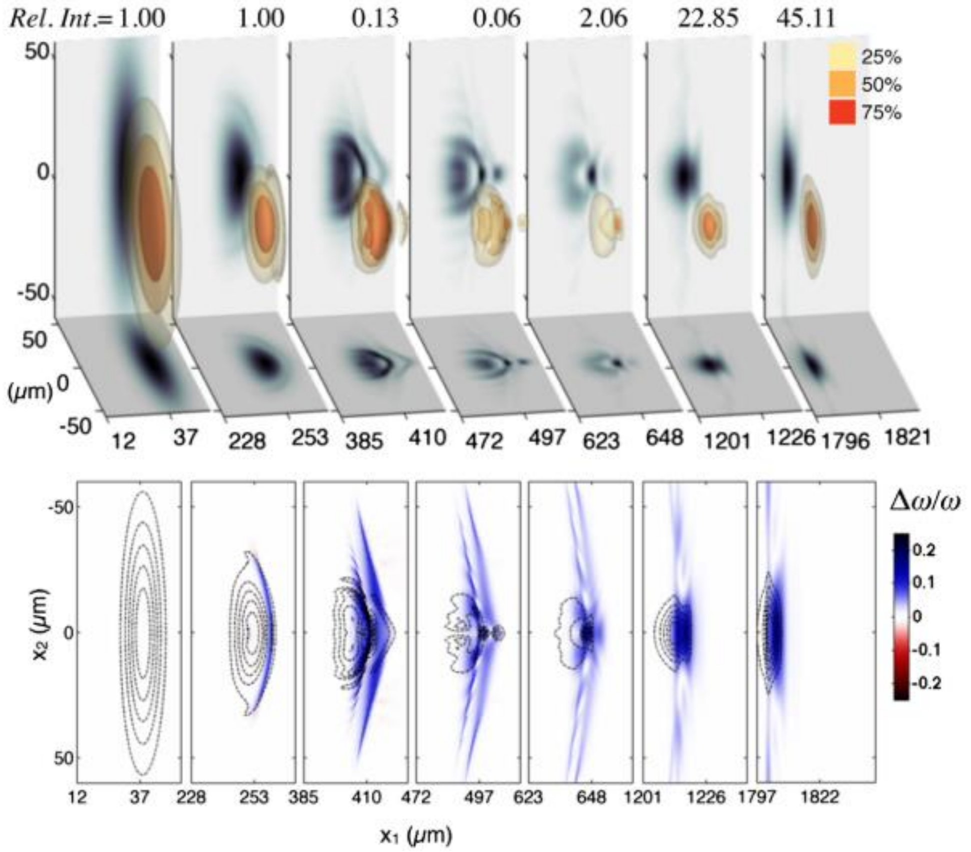

Figure 2. Top panel: isosurface plots (25%, 50%, and 75% of the maximum intensity) showing the pulse dynamics at different propagating distances. Side panels display intensity profiles at cross-sectional planes through the center of the box. Bottom panel: spatial distribution of the local frequency shift of the laser pulse for the center slice [40].

This is achieved by the combination of ionization-induced refraction, focusing, and diffraction in 3D space. The simulation indicates that the spectral broadening can be mainly attributed to optical-field-ionization. The complicated dispersion of the higher-order modes generated by the ionization gradients leads to pulse compression. Figure 2 shows the simulated pulse dynamics at different propagating distances. As the pulse converges towards the focus, the leading part of the pulse gradually becomes blue shifted due to ionization. Then the laser pulse experiences a dramatic nonlinear refraction because of the rapidly changing refractive index induced by the increasing electron density. In this process, a dynamic redistribution of the pulse energy takes place, which leads to not only an enhanced peak intensity, but also a shorter temporal duration. In a recent work, self-compression of 98 fs near-infrared laser pulses down to 8.8 fs was demonstrated in ambient air through conical radiation [41]. The self-compression can also occur in air under conditions of no ionization. Utilizing the anomalous dispersion of air from 3.5 to 4.2 μm, self-compression of high peak power pulses are achieved by loosely focusing the beam in air [42]. Besides soliton effects, the strong higher order dispersion near the edge of the CO_2 absorption band affects the soliton dynamics.

2.3 Filaments

A laser pulse with peak power above the critical power should undergo a collapse because of self-focusing. However, when the beam becomes sufficiently intense, a plasma is generated near the collapse location, which defocuses the beam core. Once defocused, the beam may still contain a power above critical value and undergo another focusing-defocusing cycle. The repetition of this scenario sustains a long range, self-guided propagation in the form of a filament. The filamentation is not only good for laser beam guiding and long-distance propagation, but also useful in pulse shortening. 5.7 fs, 0.38 mJ pulses with an excellent spatial beam profile were generated in filamentations in Ar gas by Hauri et. al. [43]. In this work, they compressed the pulses in a two gas cell configuration. Near single-cycle pulses generated by filamentation in noble gas were predicted in [44]. Stibenz et. al. demonstrated self-compression of mJ pulses to 7.8 fs duration in a Kr filamentation without the need for any additional dispersion compensation [28]. Although self-compression by filamentation has the potential to generate near single-cycle pulses, its energy scaling is limited by the multi-filamentation. To get good self-compression and beam profile, the self-compression usually needs to operate in the single filament regime.

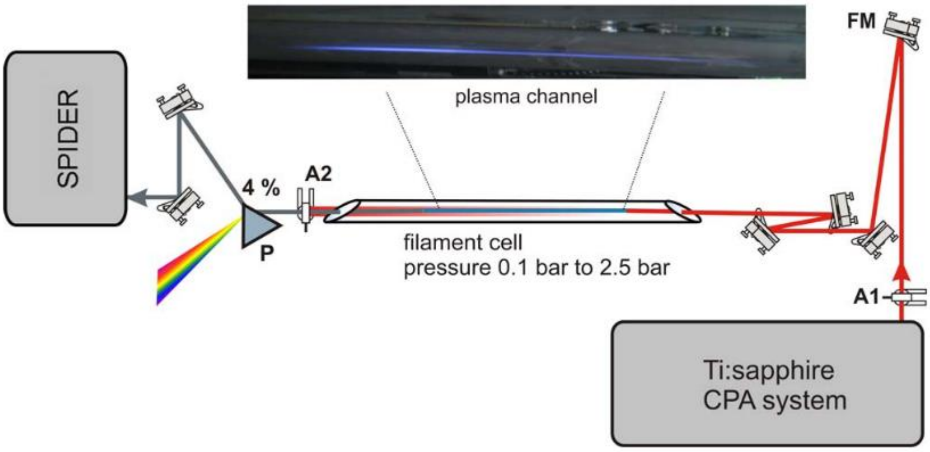

Figure 3. The typical experimental set up for self-compression of laser pulses by filamentation [45].

Figure 3 shows a typical experimental set up for self-compression of laser pulses by filamentation. The high-power laser is focused into a gas cell fill with noble gas and forms the filamentation. The pressure inside the gas cell can be finely tuned to get the optimal compression. There is also an aperture before the gas cell to control the filamentation. Usually, the pulses after the gas cell are already self-compressed and there is no need for any post compression stage. However, the optics after the gas cell (e.g., windows) can induce some chirp, in which case, a post compression setup may be necessary to get near Fourier transform pulses. With the help of chirped mirrors, few-cycle high energy pulses were generated in two-stage filamentations [43, 46, 47].

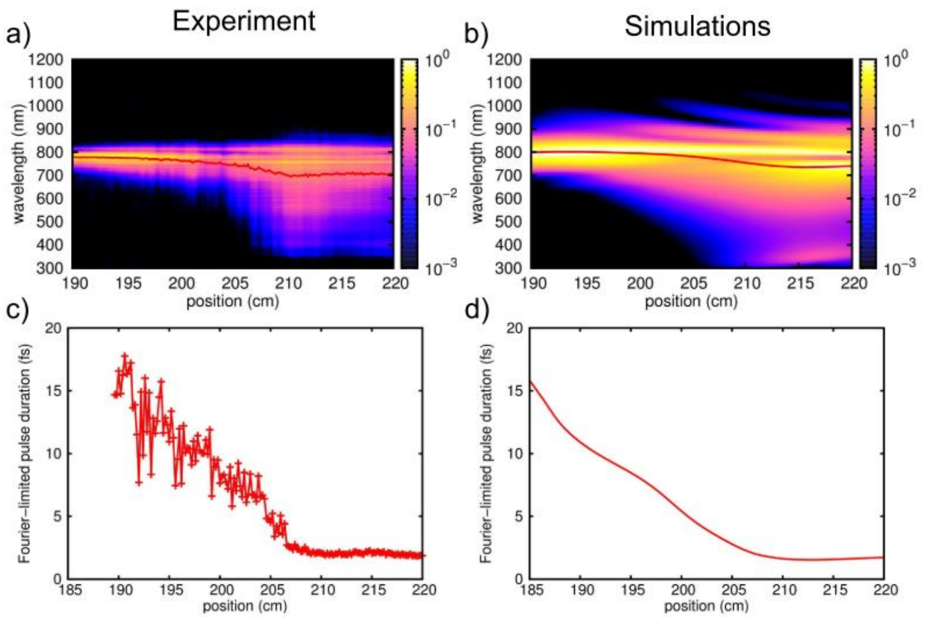

Figure 4. The measured (a) and simulated (b) spectrum along the propagation direction of the filament. The red lines are the central frequency along the propagation. (c) and (d) are the Fourier-limited pulse duration determined from the spectra [48].

Direct experimental observation of self-compression along a filament was reported by Kretschmar et. al. [48]. They designed the set up with an adjustable focal spot position inside a semi-infinite gas cell to measure the filamentation dynamics along the propagation direction. A significant spectral broadening is observed with ongoing propagation of the filament as seen in Figure 4(a). The Fourier-limited pulse duration approached ~2.5

fs which corresponds to a single cycle at the wavelength of 800 nm. This direct measurement inside the filament helps study the complex dynamics occurring along filamentary propagation and contribute to the understanding of nonlinear interaction along the filament. In a work by Trisorio et al., they reported the first self-compression of circularly polarized pulses in the multi-filamentation regime [49]. Compared with linearly polarized pulse generating multi-filamentation, an enhancement in spatial stability and energy throughput was demonstrated with circular input polarization. This enhancement benefits from the fact that circularly polarized light has lower Kerr nonlinearity and higher critical power for self-focusing [50]. With the initial 57 fs laser pulse duration, 11.9 fs and 15.2 fs pulses were measured in the two co-propagating filaments after compression by a 20 mm-thick fused silica (see Figure 5(c) and (d)). This work explored the potential of multi-filamentation for providing a stable multi-beam, high energy, few-cycle pulse source to overcome the energy limitation given by the single filament approach. Although self-compression by filamentation has many advantages such as high energy and few-cycle pulse durations, they often suffer from large spatial inhomogeneity of their spectrum. The optimum compressed pulses are normally achieved only in the central area.

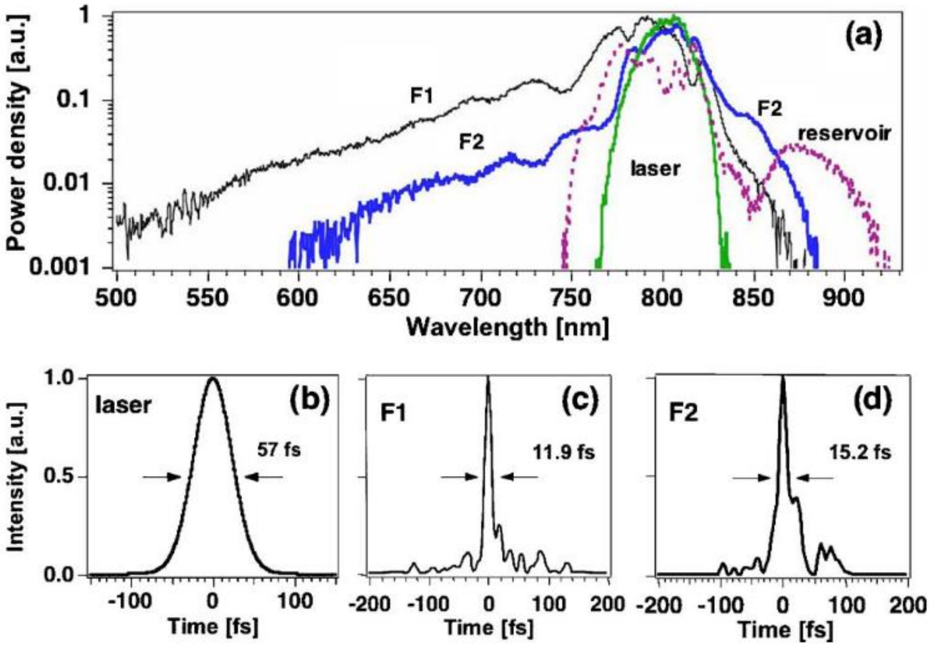

Figure 5. (a) Spectra of the laser and the circularly polarized twin filaments F1 and F2. The spectrum of the reservoir radiation is measured in the geometrical center of the twin filaments. The temporal reconstruction of (b) the initial laser and (c), (d) the two co-propagating filament pulses after compression by a 20 mm-thick fused silica are also shown [49].

3. Self-compression in waveguides

There are two advantages of using waveguides for self-compression: (i) the pulses in a waveguide can propagate an extended length while maintaining their beam size and thus intensity. These propagation lengths normally exceed the Rayleigh length of the focusing by orders of magnitude. This increases the interaction length and results in extended spectral broadening for shorter pulses. (ii) The propagation of pulses in a waveguide is in the form of eigenmodes which lead to a coherent mixing of different spatial parts of the beam. The eigenmodes exhibit the same spectral and temporal behavior over the entire beam profile. Therefore, self-compression in waveguides can get better compressed beam profiles compared with those in free propagation. Figure 6 illustrates the different phases of a typical self-compression in waveguide.

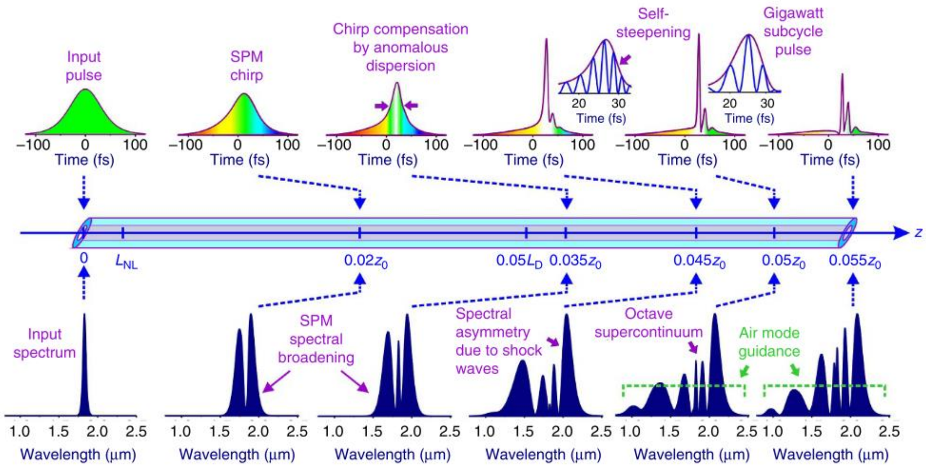

Figure 6. Different phases of the pulse self-compression in a waveguide [51].

3.1 Hollow Core Photonic-Crystal Fibers

Soliton self-compression as commonly implemented in solid-core fiber [52-54] is also suitable in hollow core photonic-crystal fibers (HC-PCF) when the pulse energy is increased. Soliton self-compression relies on the cyclic propagation behaviour of higher-order solitons in hollow core PCF in the anomalous dispersion regime. In these conditions, spectral broadening and simultaneous temporal compression can be exploited once a proper length of the medium is chosen. The relative strength of nonlinearity with respect to dispersion is characterized by the soliton order $N = \sqrt{L_d/L_{SPM}}$, where $L_d = T_0^2/\beta_2$ is the dispersion length, T_0 is the input pulse duration, β_2 is the group velocity dispersion (GVD), and L_{SPM} is the characteristic length for self-phase modulation (SPM) [55]. Soliton self-compression is possible for propagation at soliton orders $N > 1$. The compression ratio and quality factor can be estimated as $\sim 4.6N$ and $\sim 3.7/N$ respectively from detailed analysis of a large number of numerical simulations [56, 57]. Taking both into account, a soliton order of $N \sim 4$ provides a good combination of compression characteristics with pulse durations down to 2 fs expected for typical experimental parameters in kagome PCF [58]. In 2013, Mak et al. achieved soliton self-compression from 24 to 6.8 fs at output energies of 6.6 μJ in a gas-filled hollow core kagome PCF [59] (see Figure 7). Self-compression in air filled kagome PCF from ~500 fs to 49 fs with output energy of 280 μJ was obtained by Debord et al. [60].

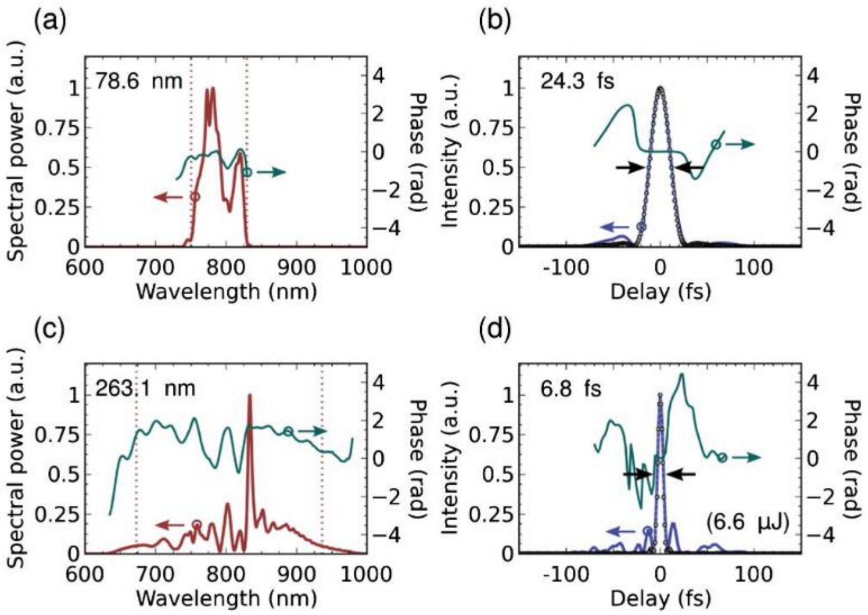

Figure 7. (a) Measured spectrum and (b) reconstructed temporal profile of input pulse based on direct measurement before the fiber-coupling lens; (c) measured output spectrum and (d) temporal profile of self-

compressed pulse after propagating through 11 cm of fiber filled with 13 bar Ne at the input and vacuum at the output [59].

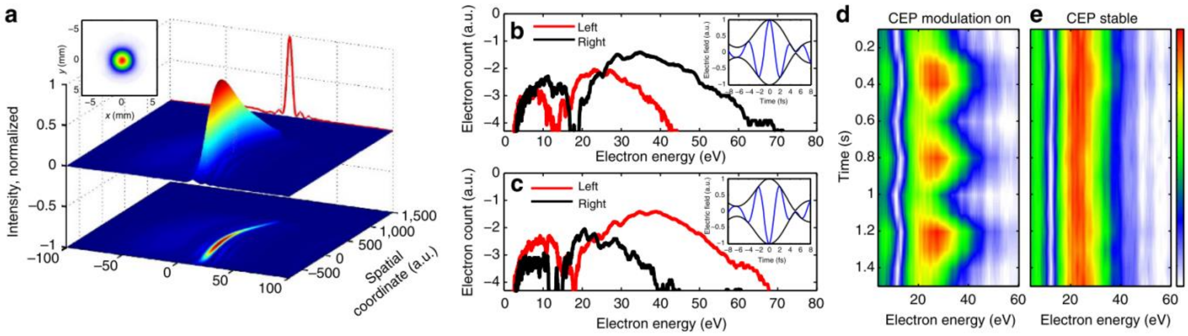

Figure 8. (a) The spatial uniformity and whole-beam compression are illustrated in the spatiotemporal reconstruction of the pulse and measured beam profile shown in the inset; (b, c) The photoelectron spectrum of ionized Xe atoms in two directions in stereo-ATI spectrometer using self-compressed pulses for +cos and –cos electric fields; (d, e) The self-compressed pulses retain the CEP phase of the much longer input pulses despite the very high compression ratio [51].

In 2015, Balciunas et al. achieved pulse self-compression down to 4.5 fs with 35 µJ pulse energy at wavelength of 1.8 µm based on shock-wave formation in an ultrabroadband kagome PCF [51]. The propagation in waveguide ensures a consistent self-compression across the entire beam cross-section, and not only around the central portion. The experimentally obtained spatiotemporal pulse intensity distribution is shown in Figure 8(a). This is one of the key strengths of such compression techniques compared with self-compression in free propagation. They also showed that the self-compressed pulses preserve the CEP phase of the input pulses. In 2017, Gebhardt et al. reported on self-compression to 34.4 µJ, 2.1-cycle pulses with 1.4 GW peak power at a central wavelength of 1.8 µm and an average power of 43 W in a gas-filled anti-resonant HC-PCF [61]. Elu et al. achieved compression close to a single cycle at an average power of 9.6 W in the mid-IR regime by applying the soliton self-compression technique in an anti-resonant HC-PCF [62]. The resulting peak power of 3.9 GW in combination with the near-single-cycle duration and intrinsic CEP stability benefits many applications in strong-field physics. By solving the generalized nonlinear Schrödinger equation which includes both the ionization and self-steepening terms, Stepanov et al. later validated the experiments by Elu et al. [62] numerically [63]. They also suggested that multioctave supercontinuum can be generated via soliton self-compression coupled with shock-wave pulse self-steepening, yielding an extraordinarily short, sub-half-cycle field transients. In 2019, Ermolov et al. generated CEP-stable 1.7 cycle pulses at 800 nm through soliton self-compression in a HC-PCF with 1 µJ single pulse energy at 800 kHz repetition rate, providing 0.8 W of average power [64]. In 2020, Kottig et al. reported soliton self-compression to single-cycle durations with 5 µJ output pulse energy at 9.6 MHz repetition rate in a neon-filled anti-resonant HC-PCF [65] (see Figure 9). In a recent paper by Savitsky et al., sub-cycle pulse at central wavelength of 1.8 µm was achieved through soliton self-compression in an argon-filled anti-resonant HC-PCF [66].

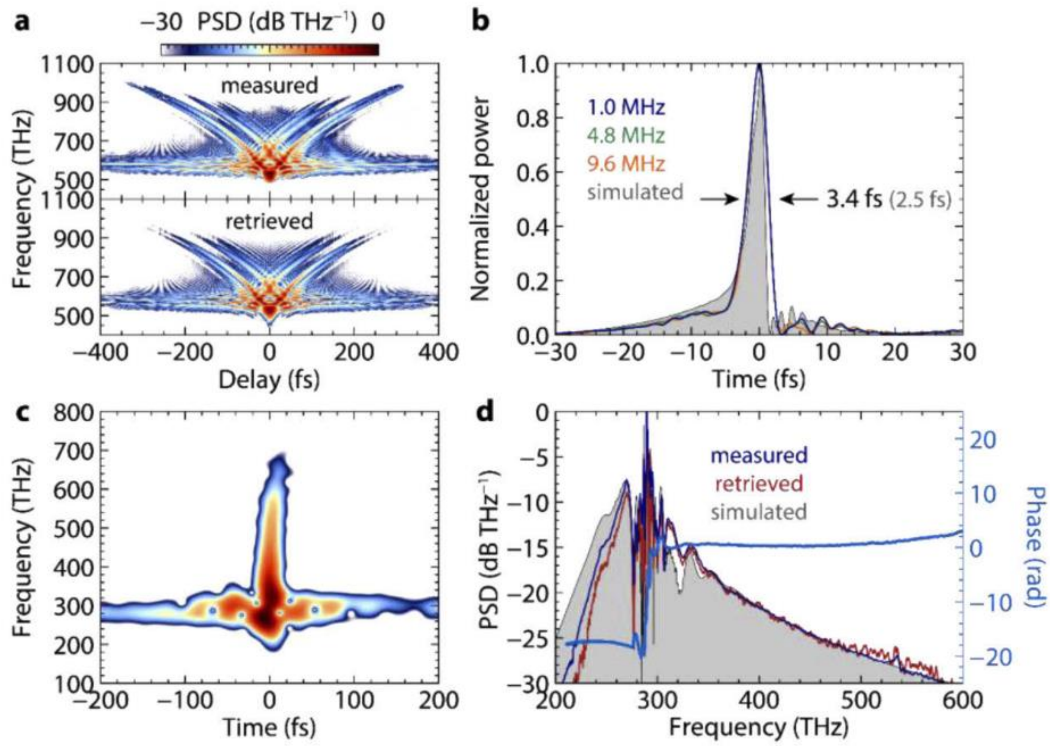

Figure 9. (a) The measured and retrieved SHG FROG traces at 9.6 MHz repetition rate. (b) Retrieved pulses at repetition rates of 1, 4.8 and 9.6 MHz, numerically back-propagated to the fiber output. (c) Spectrogram of the pulse at 1 MHz repetition rate, calculated with a 15 fs Gaussian gate pulse. (d) Directly measured spectrum and FROG-retrieved spectrum and phase of the pulse at 1 MHz repetition rate [65].

3.2 Capillaries or simple hollow-core fibers

Capillaries or simple hollow core fibers (HCF) are different from hollow core photonic-crystal fibers. Light propagates in capillaries or simple hollow-core fibers by grazing incidence reflections and only leaky modes are supported because of power losses through the fibers' walls. Simple hollow-core fibers with larger core diameter have higher damage threshold and can manage mJ level pulses. In 2004, Wagner et al. demonstrated a self-compression from 30 to 13 fs by propagating mJ pulses inside a hollow core waveguide filled with low-pressure argon gas [26]. The waveguide effect of HCF can play a very important role in the self-compression phenomenon. They said that the compression levels became weak when using a larger diameter capillary and the compression disappeared when the waveguide was replaced by a large-diameter cell [26]. On the other hand, there are other papers reporting that self-compression relies on multimode coupling inside the capillary. In [67], the spatiotemporal compression of energetic femtosecond laser pulses within gas-filled fibers was examined using a pulse propagation model based on a multimode generalized nonlinear Schrodinger equation (see Figure 10). In their study the plasma defocusing, and linear propagation effects are also included and shown to be the dominant processes within a highly dynamical mechanism that enables 100 fs pulses to be compressed down to the few-cycle regime after less than 50 mm of propagation. Another self-compression mechanism using HCF was claimed by the generation of a thin plasma column in the center of the fiber [68]. They showed that a few cm long, homogeneous, plasma column with an electron density of the order of 10^{17} cm^{-3} is created for an incident intensity of 4×10^{15} W/cm^2. In 2009, Skobelev et al. demonstrated self-compression of a laser pulse from 76 to 40 fs by propagating in a gas-filled hollow dielectric capillary [69]. The nonlinear plasma channel generated inside the capillary provides strong anomalous dispersion and confinement for effective self-compression of an optical pulse. Their simulation showed that a laser pulse shorter than 10 fs can be generated in the optimal regime with the energy efficiency exceeding that of self-compression in a filament (see Figure 11). At the same time, the compression in their simulation is uniform over the beam cross section, which indicates a quasi-single-mode regime of radiation propagation in the nonlinear plasma waveguide. Finally, this kind of ionization compression scheme has very weak upper constraints in the energy of the initial laser pulse and, according to the numerical simulation, is applicable for pulse energies of tens of millijoules.

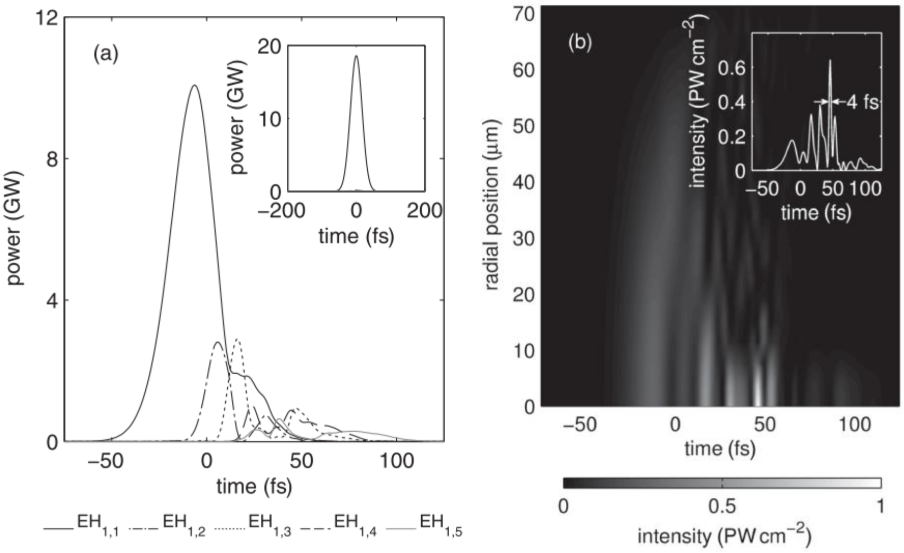

Figure 10. (a) Modal pulse envelopes at the exit of a 50-mm section of hollow fiber filled with 100 mbar of argon. The inset shows the envelopes of the 40 fs pulse at the launch. (b) Spatiotemporal field at the output constructed from these envelopes and their transverse spatial mode functions [67].

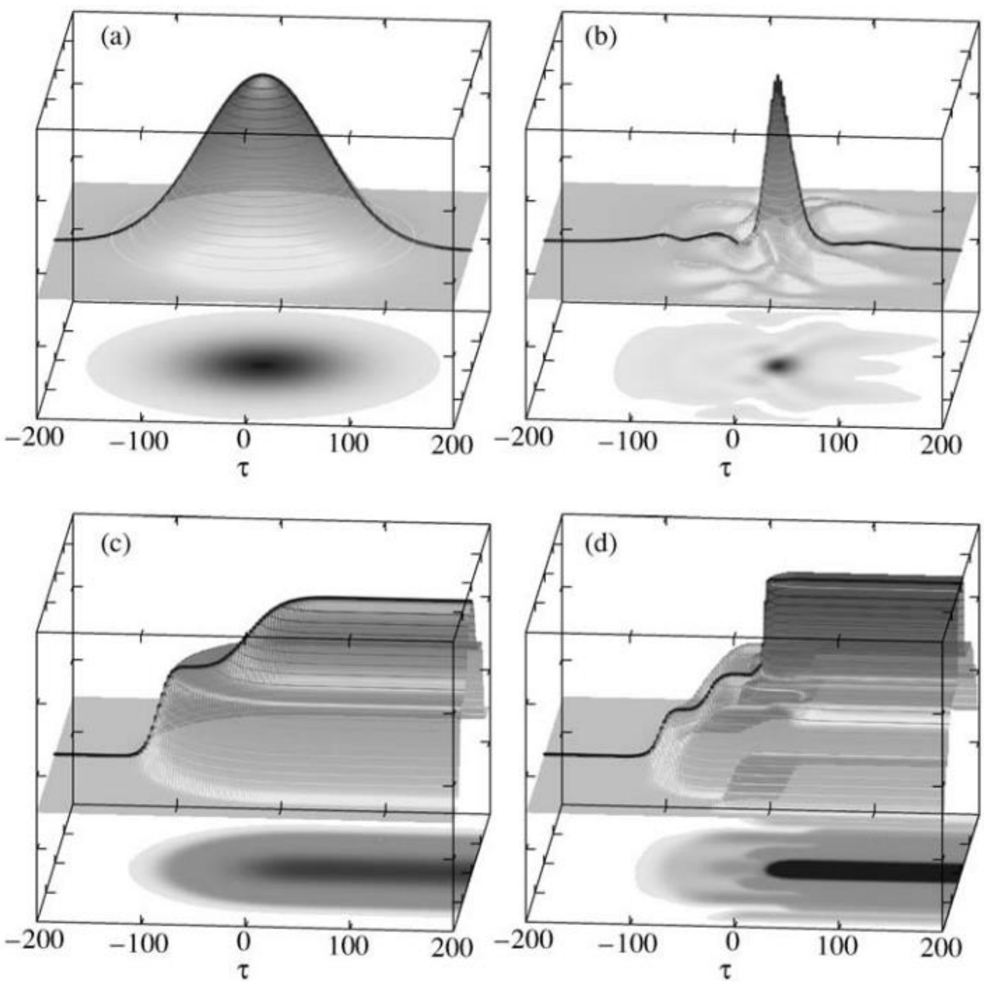

Figure 11. Simulated spatial-temporal distributions of the pulse intensity and plasma density at the (a, c) input and (b, d) output of a 3.6 cm long capillary [69].

In the simulation plasma defocusing causes a considerable quantity of power to be coupled to high-order modes where negative waveguide dispersions are present. Therefore, linear propagation effects lead to redistribution of the pulse energy temporally in high-order modes. Eventually, the dynamically compressed pulses are achieved at the end of the capillary when all the waveguide modes are combined. Besides ionization induced self-compression, soliton self-compression phenomenon was also found in simple hollow core fibre. For simple hollow core waveguide, the soliton fission length which approximates the required length scale for soliton self-compression and subsequent pulse breakup can be calculated as [32]

$$L_{fiss} \approx \frac{a^2\tau_{fw}^2}{3N|\delta(\lambda_0,\lambda_{zd})|} \propto \frac{a^2\tau_{fw}}{\sqrt{I_0}}, \tag{3}$$

where a is the inner core radius, τ_{fw} is the FWHM pulse duration, N is the soliton order number, I_0 is the peak intensity, $\delta(\lambda_0, \lambda_{zd})$ is a function that describes the dispersion of the filling gas, λ_0 is the laser wavelength, and λ_{zd} is the zero-dispersion wavelength. By using large core, simple HCFs of long lengths and shorter pump pulses, Travers et al. observed soliton self-compression to sub-cycle pulses with 43 GW peak power and inferred the creation of sub-femtosecond field waveforms [32]. With a similar approach, Brahms et al. coupled 1800 nm laser pulses with a FWHM duration of 30 fs into a 2.5 m long argon filled simple HCF with an inner diameter of 450 um and achieved the compressed pulse with a FWHM duration of only 2 fs [70] (see Figure 12). The soliton self-compression is more applicable for mid-IR sources because of negative dispersion properties of simple HCFs in those wavelength ranges.

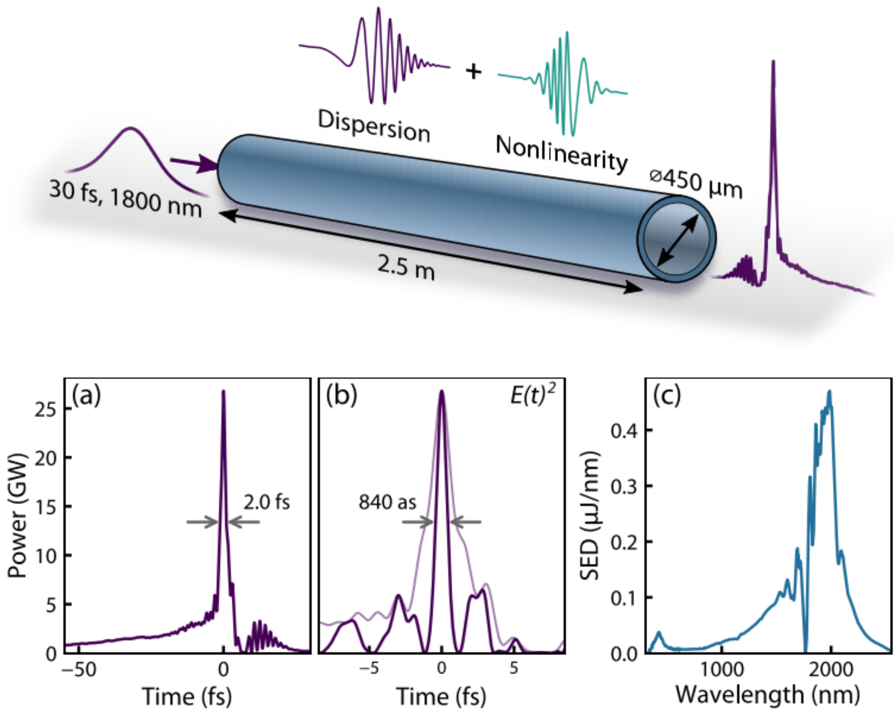

Figure 12. (a) The temporal profile of the pulse at the HCF exit which corresponds to an 840 as field transient (b). The spectrum of this pulse extends from the ultraviolet to the mid-IR (c) [70].

4. Mechanisms behind laser pulse self-compression

Based on the mechanisms involved, we divide reports on pulse self-compression into three categories: self-compression by filamentation, ionization-induced self-compression, and soliton self-compression. To further analyze these reports on self-compression of laser pulses, we calculate the input peak powers and critical powers in these reports and plot them in Figure 13. The green line is where the input peak power equals to the critical power, $P_{in} = P_{cr}$. We can identify that all the self-compression by filamentation works fall in the region where $P_{in} > P_{cr}$, since this is a requirement for filamentation. For $P_{in} > P_{cr}$, self-focusing occurs, and dominates diffraction, which leads to collapse of the beam [71, 72]. The collapse dynamics are dictated by the shock formation due to space-time focusing and self-steepening as discussed in [72].

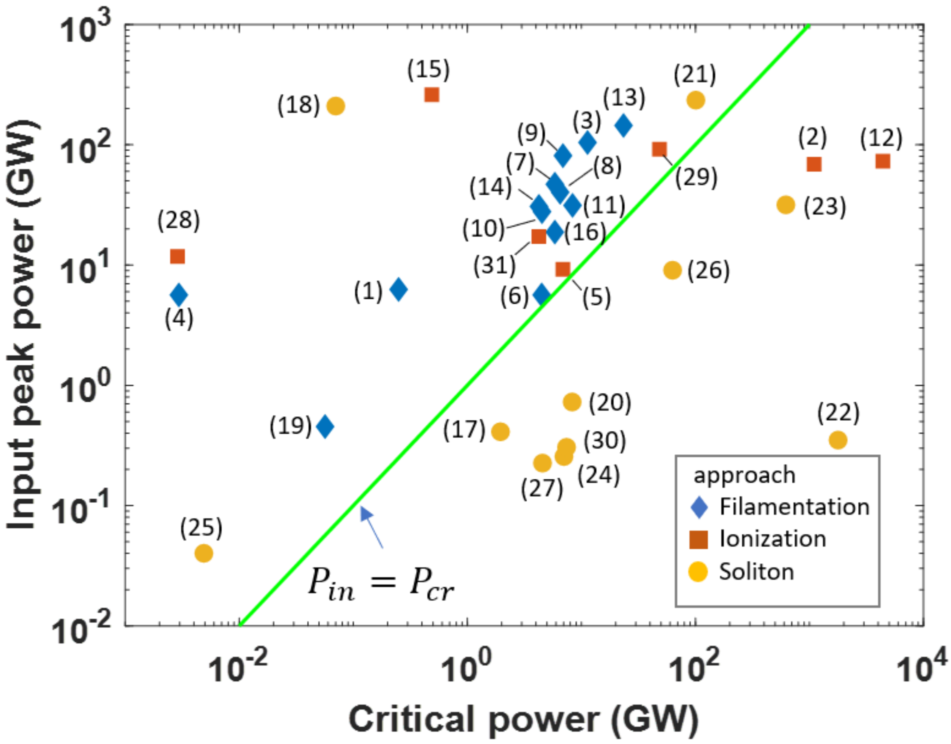

1. Koprinkov et al. 2000 [25]
2. Wagner et al. 2004 [26]
3. Stibenz et al. 2006 [28]
4. Chen et al. 2006 [35]
5. Chen et al. 2007 [74]
6. Hauri et al. 2007 [75]
7. Trunov et al. 2007 [76]
8. Akturk et al. 2008 [77]
9. Kurilova et al. 2009 [79]
10. Mucke et al. 2009 [81]
11. Schulz et al. 2009 [45]
12. Skobelev et al. 2009 [69]
13. Otsuka et al. 2010 [84]
14. Varela et al. 2010 [86]
15. He et al. 2014 [40]
16. Kretschmar et al. 2014 [48]
17. Balciunas et al. 2015 [51]
18. Shumakova et al. 2016 [39]
19. Marcinkeviciute et al. 2017 [73]
20. Elu et al. 2017 [62]
21. Mitrofanov et al. 2017 [42]
22. Gebhardt et al. 2017 [61]
23. Travers et al. 2019 [32]
24. Maurel et al. 2019 [78]
25. Grobmeyer et al. 2020 [80]
26. Brahms et al. 2020 [82]
27. Kottig et al. 2020 [65]
28. Gao et al. 2021 [83]
29. Ran et al. 2022 [85]
30. Savitsky et al. 2023 [66]
31. Xie et al. 2023 [41]

Figure 13. The input peak powers are plotted versus the critical powers for past works on self-compression of laser pulses.

In a real medium, the collapse can be arrested by various mechanisms such as GVD [87-89], saturation of nonlinear refractive index [90, 91], nonlinear losses [92, 93]. The relevant mechanism for the arrest of collapse before filamentation in air is multi-photon absorption and its associated plasma-defocusing. The laser beam will self-focus first then the intensity becomes sufficiently high for multiphoton ionization. A plasma is generated near the collapse location, which defocuses the beam. The defocused beam may still have a power above critical value and undergo another focusing-defocusing cycle. The repetition of this scenario sustains a long range, self-guided propagation in the form of a filament. White light generation was reported to occur during the propagation of ultrashort laser pulses undergoing filamentation in condensed media as well as in gases [94-96]. These white light generation processes are normally coherent. The generated broad spectrum can support few-cycle and even single-cycle pulses. Calculations by Couairon et al. predict that filamentation in gas with pressure gradient generates single-cycle pulses with pulse energy of several hundreds of µJ [27].

The mechanisms involved in filamentation which result in self-compression are summarized in Figure 14. In the beginning, space-time focusing and self-steepening dictate the collapse dynamics and a steep edge is formed at the back of the pulse (i.e., optical shock wave). This initial process directly leads to the pulse shortening and peak intensity increase. This is followed by multiphoton ionization and plasma formation that arrest the collapse when the powers significantly exceed the threshold for collapse. This forms a self-guided filament, and supercontinuum generation takes place along the propagation. On the other hand, the plasma formation provides a negative GVD which contributes to the compression of the supercontinuum generated. In fact, Hauri et al. showed that filaments carrying strong negative chirp are generated, which allow easy temporal compression by chirp compensation in any normally dispersive elements [97].

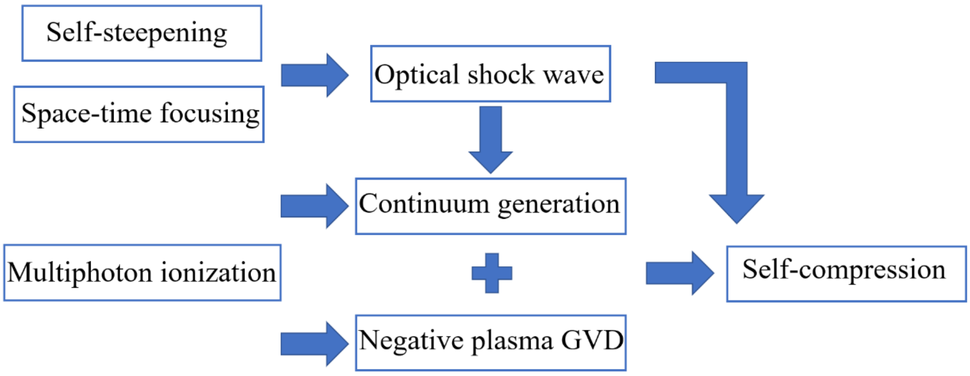

Figure 14. Mechanisms involved in filamentation resulting in self-compression.

Although $P_{in} > P_{cr}$ is required for self-compression by filamentation, this requirement is not necessary for self-compression by ionization as shown in Figure 13. In self-compression by ionization, low density gases are often used. This enhances the power efficiency. The idea of ionization self-compression was first introduced in Ref. [98], where it was shown that ionization-induced chirps can be compensated in plasma, thus leading to pulse compression. The key idea is the use of such gas density that the conditions of single-mode propagation can be violated, and an ionization-nonlinear plasma waveguide can be formed. Strong anomalous dispersion of such a nonlinear plasma waveguide can lead to the effective self-compression of an optical pulse. The condition of violating the single-mode radiation propagation regime (i.e., going into effective ionization self-compression regime) in the hollow core waveguide has the form [24]

$$\rho_0 > \frac{mc^2}{4\pi e^2}\frac{u_{12}^2 - u_{11}^2}{a^2} \tag{4}$$

where ρ_0 is the initial density of neutral gas atoms, $u_{11} = 2.405$ and $u_{12} = 5.52$ are the first and second zeros of the zeroth-order Bessel function, respectively, e is the electron charge, m is the electron mass, c is the speed of light, and a is the radius of the waveguide inner core.

Most self-compressions by solitons are operated in the $P_{in} < P_{cr}$ regime as shown in Figure 13. The self-compression by solitons is normally operated in HC-PCFs with anomalous dispersions. The spectral broadening is achieved through SPM induced by Kerr effect of gas atoms filled in the HC-PCFs. The positive dispersion accumulated in the SPM process is balanced by the anomalous waveguide dispersion, the solitons are then formed. The $P_{in} < P_{cr}$ requirement ensures that the beam propagation inside the hollow core PCFs in the fundamental mode and avoids ionization by self-focusing effects. There are three exceptions in Figure 13 [number (18), (21) and (25)]. These cases, however, do not involve HC-PCFs, and are discussed one by one in the following paragraphs.

In the work by Shumakova et al., although the input peak power is more than three order of magnitudes higher than critical power, they achieved soliton self-compression in a mm thin YAG [39]. The YAG was too thin to form filamentation inside by self-focusing effects. The three-dimensional numerical modelling in their paper reveals that under their operating conditions, the length of temporal compression is much shorter than the length of spatial modulation instability and beam breakup into multiple filaments. It is exactly this separation of length scales attainable in the regime of strong anomalous dispersion of MIR pulses that allows the use of a solid medium for temporal compression at such high input peak powers.

Mitrofanov et al. demonstrated that high peak power MIR pulses can be soliton self-compressed during free propagation within the regions of anomalous dispersion in air to yield few-cycle sub-terawatt field waveforms [42]. The input peak power is estimated to be larger than the critical power, but they confirmed that there were no filamentations, and explained the self-compression by soliton dynamics with influence of higher order dispersion (HOD). Grobmeyer et al. put a thin fused silica inside a multi-pass cell to operate soliton self-compression [80]. The nonlinearity is accumulated over many passes each of which induced a small amount of nonlinear phase. In this way, nonlinear propagation in the medium is a small perturbation to free propagation in space and self-focusing to beam collapse can be avoided even in the regime of $P_{in} > P_{cr}$.

In summary, self-compression of laser pulses can also be classified into four regimes by comparing the peak power (P_{in}) and peak intensity (I_{in}) of the input pulse to the critical power of self-focusing (P_{cr}) and the ionization threshold intensity of the nonlinear medium (I_{th}) respectively. The classification is shown in Table 1.

Table 1. Self-compression of laser pulses in different power and intensity regimes.

	$P_{in} > P_{cr}$	$P_{in} < P_{cr}$
$I_{in} > I_{th}$	Self-compression by filamentation [28, 45, 48, 73, 75-77, 79, 81, 84, 86]	Self-compression by ionization [26, 40, 41, 69, 74, 83, 85]
$I_{in} < I_{th}$	Self-compression by self-focusing [25, 35]	Self-compression by solitons [32, 39, 42, 51, 61, 62, 65, 66, 70, 78, 80]

5. State-of-the-art

In this section we summarize the past works on self-compression of high energy laser pulses and compare them on four figures-of-merits: compressed pulse duration, pulse energy, peak power, and average power. We first classify them into three main categories based on the laser sources used: Ti:sapphire lasers, which have been the workhorse of ultrafast science in the last decades; ytterbium-doped (Yb) high-power lasers; and the secondary laser sources based on optical parametric amplification (OPA) or optical parametric chirped pulse amplification (OPCPA) that are normally in the mid-IR range. Additionally, we divide them into three classes depending on the mechanisms of self-compression as discussed in the previous sections: filamentation, ionization-induced, and soliton self-compression. These works are summarized and plotted in Figure 15 and 16. We observe that for almost all reports that used the soliton self-compression, the pulse energies are below 0.3 mJ. This is because they are normally achieved in the hollow core capillary or hollow core photonic crystal fibers which have small damage thresholds. There are two exceptions to this. One is achieved by soliton self-compression in a mm-long yttrium aluminum garnet crystal [39], and the other is in anomalously dispersive air [42]. The laser wavelengths used by these two works were 3.9 um, at which most materials exhibit anomalous dispersion. Most reports on the soliton self-compression are achieved by Yb laser, OPA or OPCPA laser sources. The only report on soliton self-compression using Ti:sapphire laser is by Travers et al. [32]. They reported the soliton self-compression in hollow core capillary by applying shorter pump pulses and longer HCF. They achieved the shortest compressed pulse of all works which is only 1.2 fs wide. We can see that only soliton self-compression can reach very short pulse durations (<5 fs), although their pulse energy tends to be relatively small. The highest peak power achieved for 800 nm Ti:sapphire laser is by ionization-induced self-compression in a gas jet by He et al. [40]. The highest pulse energy and peak power were achieved through soliton self-compression in a 2-mm thick YAG by Shumakovaet al. [99]. The highest average power was achieved by Grobmeyer et al. through putting a thin fused silica inside a multi-pass cell to operate soliton self-compression [80]. The second highest average power was achieved by soliton self-compression in an anti-resonant HC-PCF by Kottig et al. [65].

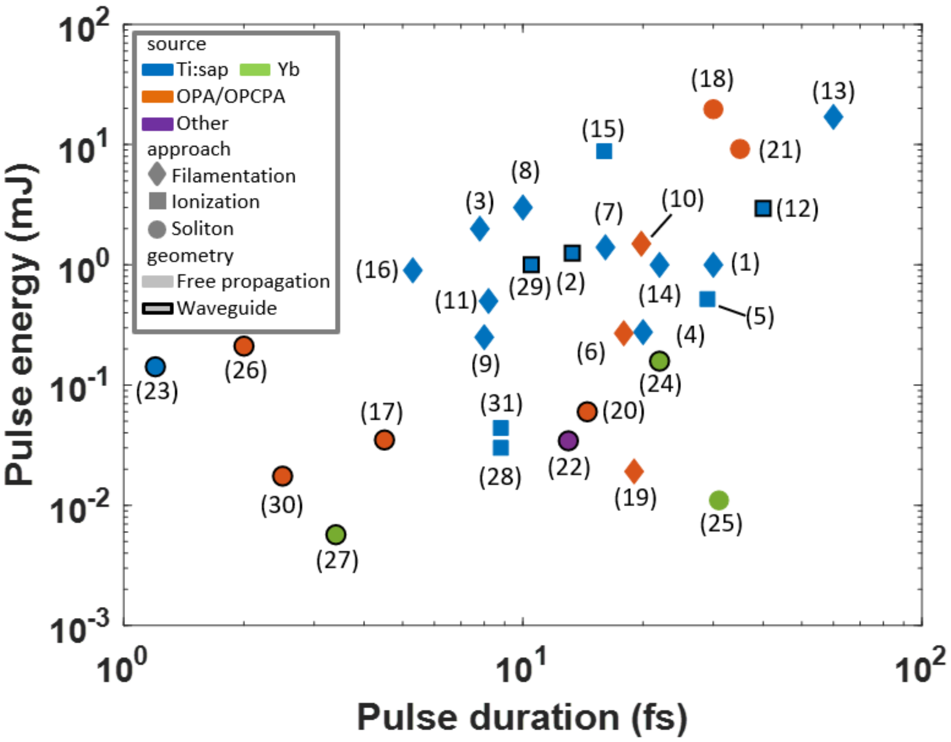

1. Koprinkov et al. 2000 [25]
2. Wagner et al. 2004 [26]
3. Stibenz et al. 2006 [28]
4. Chen et al. 2006 [35]
5. Chen et al. 2007 [74]
6. Hauri et al. 2007 [75]
7. Trunov et al. 2007 [76]
8. Akturk et al. 2008 [77]
9. Kurilova et al. 2009 [79]
10. Mucke et al. 2009 [81]
11. Schulz et al. 2009 [45]
12. Skobelev et al. 2009 [69]
13. Otsuka et al. 2010 [84]
14. Varela et al. 2010 [86]
15. He et al. 2014 [40]
16. Kretschmar et al. 2014 [48]
17. Balciunas et al. 2015 [51]
18. Shumakova et al. 2016 [39]
19. Marcinkeviciute et al. 2017 [73]
20. Elu et al. 2017 [62]
21. Mitrofanov et al. 2017 [42]
22. Gebhardt et al. 2017 [61]
23. Travers et al. 2019 [32]
24. Maurel et al. 2019 [78]
25. Grobmeyer et al. 2020 [80]
26. Brahms et al. 2020 [82]
27. Kottig et al. 2020 [65]
28. Gao et al. 2021 [83]
29. Ran et al. 2022 [85]
30. Savitsky et al. 2023 [66]
31. Xie et al. 2023 [41]

Figure 15. The compressed pulse energy is plotted versus the pulse duration for the past works on self-compression of high energy laser pulses.

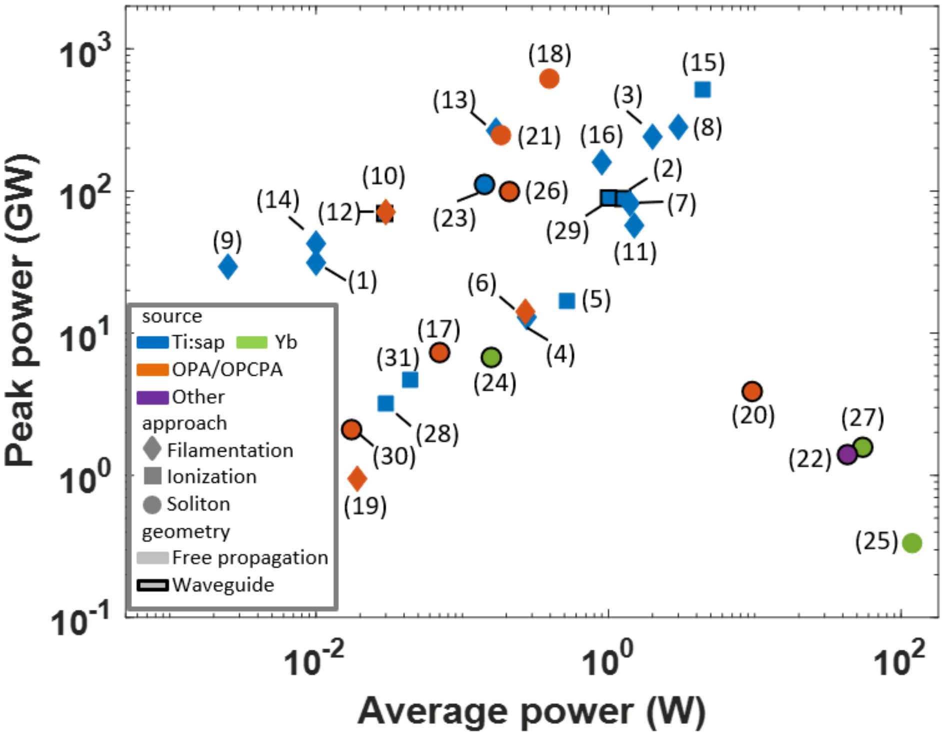

1. Koprinkov et al. 2000 [25]
2. Wagner et al. 2004 [26]
3. Stibenz et al. 2006 [28]
4. Chen et al. 2006 [35]
5. Chen et al. 2007 [74]
6. Hauri et al. 2007 [75]
7. Trunov et al. 2007 [76]
8. Akturk et al. 2008 [77]
9. Kurilova et al. 2009 [79]
10. Mucke et al. 2009 [81]
11. Schulz et al. 2009 [45]
12. Skobelev et al. 2009 [69]
13. Otsuka et al. 2010 [84]
14. Varela et al. 2010 [86]
15. He et al. 2014 [40]
16. Kretschmar et al. 2014 [48]
17. Balciunas et al. 2015 [51]
18. Shumakova et al. 2016 [39]
19. Marcinkeviciute et al. 2017 [73]
20. Elu et al. 2017 [62]
21. Mitrofanov et al. 2017 [42]
22. Gebhardt et al. 2017 [61]
23. Travers et al. 2019 [32]
24. Maurel et al. 2019 [78]
25. Grobmeyer et al. 2020 [80]
26. Brahms et al. 2020 [82]
27. Kottig et al. 2020 [65]
28. Gao et al. 2021 [83]
29. Ran et al. 2022 [85]
30. Savitsky et al. 2023 [66]
31. Xie et al. 2023 [41]

Figure 16. The compressed peak power is plotted versus the average power for the past works on self-compression of high energy laser pulses.

6. Conclusion and outlook

Few-cycle high energy pulses are becoming very important in nonlinear optics and strong-field physics. The traditional methods to obtain them are post compression techniques such as the spectral broadening in HCF followed by dispersive optics. However, the dispersive optics are often limited by the power damage threshold and operation bandwidth. Self-compression techniques are highly promising for achieving the shortest optical pulses down to the sub-cycle regime with multi-octave-spanning spectra which are quite challenging for post compression techniques. We reviewed different types of self-compression techniques including ionization-induced self-compression, self-compression by filamentation and solitons. Self-compression techniques by ionization and filamentation have a promising outlook in the pulse energy and power scaling although some of them suffer from poor beam qualities. The recent development of HC-PCF technologies allows higher transmission power over a broad bandwidth, as well as precise control of the dispersion profile. This makes the HC-PCF a promising platform for staging the high energy few-cycle or single to sub-cycle pulse generation with good beam quality. The next challenge is to further increase the power damage threshold of the HC-PCF. Therefore, the future direction may be a combination of these self-compression techniques. Four specific research directions are listed for future studies in the following.

6.1 Dispersion control

Higher order dispersions become more important as the pulse compresses down to the single- or sub-cycle regime. Therefore, more precise control of the input pulse dispersion is necessary. For example, Ran et al., have shown that self-compression of mJ pulsese to 10 fs was achieved by controlling the higher-order dispersion of input pulses [85]. The self-compression is optimized through finely tuning the input pulse group delay dispersion and third order dispersion. In most self-compression experiments, the input pulse spectral phase is controlled by an acousto-optic programmable dispersive filter (AOPDF) [100, 101]. The spectral phase can also be controlled by programmable Fourier transform pulse shaping which employs a number of different programmable masks or spatial light modulator (SLM) technologies, including liquid crystal SLM [102-104] and acousto-optic modulator (AOM) [105]. In recent years, dielectric metasurfaces have become a promising technology for arbitrary control of the amplitude, phase, and polarization of laser beam for spatial-domain wavefront manipulation [106, 107]. They are normally ultrathin, planar optical elements composed of an array of dielectric nanostructures. These new technologies can be implemented in the self-compression techniques for more accurate spectral phase control.

6.2 Gas mixing

For the self-compression of laser pulses in hollow core waveguides filled with noble gas, only instantaneous Kerr effect and ionization are considered in the nonlinear term. However, the Raman response must also be included for molecular gases. The nonlinear refractive index of molecular gas can be written as

$$\Delta n = n_2(1-f)I + n_2\frac{f}{\tau_0} \times \int_{-\infty}^{t} \exp\left(-\frac{t-t'}{\tau_0}\right) I(t')dt' \tag{5}$$

where f is the nonlinear refractive index ratio in the delayed component; τ_0 is the characteristic time for the delayed component; and $I(t)$ is the time dependent intensity of the pulse. The Raman response of N_2 is exploited for compression of near-infrared pulses in HCF in [108] (see Figure 17). Their experimental results and numerical simulations show that the coupling to multimode states by high energy pulses at HCF input enhances the stimulated Raman scattering process in a Raman-active medium. In ionization-induced self-compression, the ionization in noble gas only induces a strong spectral shift to the shorter wavelengths. A mixture of noble gas and molecular gas can extend both shorter and longer wavelength parts and enhance the spectral broadening for self-compression to shorter pulses.

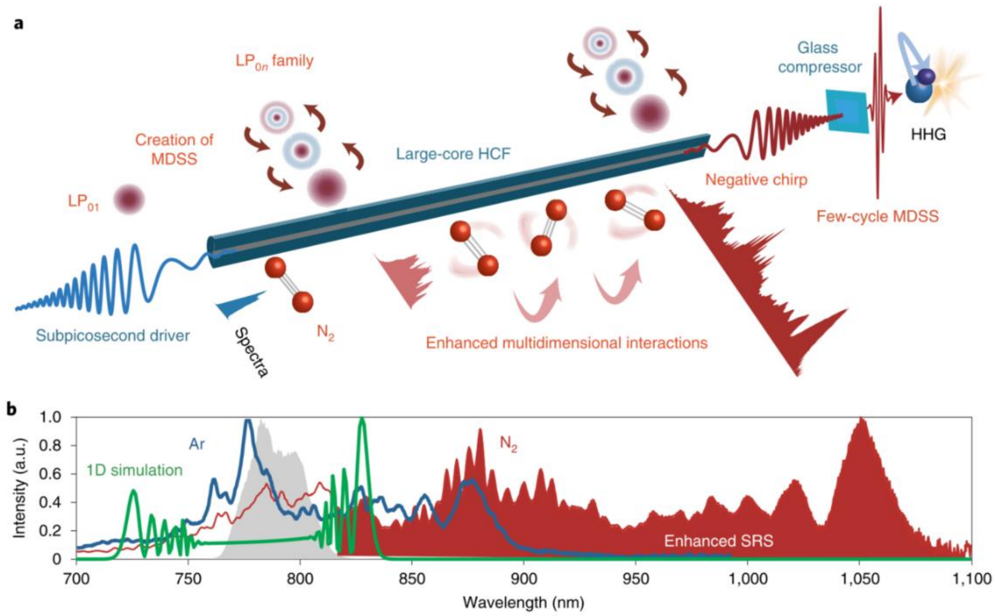

Figure 17. (a) The self-trapped multidimensional solitary states are created at the beginning of the N_2 filled HCF and propagate along it. In this process, the spectrum is largely redshifted by the enhanced cascaded stimulated Raman scattering (SRS) within the HCF as shown in (b) [108].

6.3 Fiber tapering

Tapered fibers have attracted increased interest in a variety of photonic applications such as biosensor [109], fiber lasers [110], laser beam delivery and coupling [111-114], and focusing infrared laser beams [115]. Tapered fibers with linear and exponentially-decaying profiles have been fabricated by flame brushing technique [116]. These tapered HCFs can also be applied in self-compression of laser pulses. Figure 18 shows two types of tapered hollow core waveguides which can enhance the self-compression. Type I is a tapered down waveguide. The area of the bore reduces to compensate the power loss along propagation. Type II is the opposite. The soliton pulse duration is proportional to GVD, and since the GVD decreases along the taper up fiber, the pulse duration could be compressed by adiabatic soliton effects along the taper up hollow core waveguide. The fiber tapering acts as additional tuning parameter for self-compression of laser pulses in hollow core waveguides.

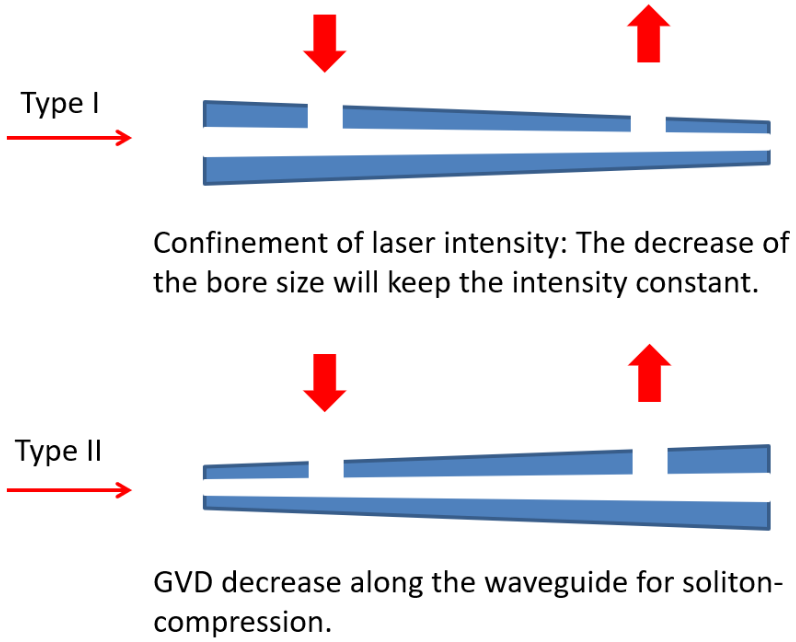

Figure 18. The tapered hollow core waveguide for laser pulse self-compression.

6.4 Higher order waveguide modes

The importance of higher order modes in laser pulse self-compression in hollow core waveguide has first been investigated by Anderson et al. [67]. The higher order mode compression has some advantages compared with the compression in fundamental mode as summarized in [117]. Firstly, the higher order modes have smaller spatial dimensions which leads to stronger nonlinearity. Secondly, the higher order modes have larger negative waveguide dispersion. This provides wider selection of gas species and pressure range which facilitate the anomalous dispersion regime for soliton self-compression. Thirdly, the larger anomalous dispersion also means that self-compression can be done within a shorter propagation length. This is critical for large-core waveguide compressors, because their bending-induced loss is one of the major limiting factors. Therefore, the higher order modes act as an additional tuning parameter for self-compression of laser pulses in hollow core waveguide. For example, Lopez-Zubieta et al. found that there always exists an optimum higher order mode for soliton self-compression, where the laser pulses can be compressed down to the single-cycle regime [118]. Higher order modes not only achieve and enhance self-compression of laser pulses, but also benefit many applications that require special spatial beam profiles.

Funding

This research is supported by A*STAR (C222812005).

References

1. Macklin, J.J., J. Kmetec, and C. Gordon III, *High-order harmonic generation using intense femtosecond pulses.* Physical review letters, 1993. **70**(6): p. 766.
2. Ghimire, S. and D.A. Reis, *High-harmonic generation from solids.* Nature physics, 2019. **15**(1): p. 10-16.
3. Li, J., et al., *Attosecond science based on high harmonic generation from gases and solids.* Nature Communications, 2020. **11**(1): p. 1-13.
4. Bai, Y., et al., *High-harmonic generation from topological surface states.* Nature Physics, 2021. **17**(3): p. 311-315.
5. Umstadter, D., et al., *Nonlinear optics in relativistic plasmas and laser wake field acceleration of electrons.* Science, 1996. **273**(5274): p. 472-475.
6. Esarey, E., C. Schroeder, and W. Leemans, *Physics of laser-driven plasma-based electron accelerators.* Reviews of modern physics, 2009. **81**(3): p. 1229.
7. Kobayashi, T., A. Shirakawa, and T. Fuji, *Sub-5-fs transform-limited visible pulse source and its application to real-time spectroscopy.* IEEE Journal of selected topics in quantum electronics, 2001. **7**(4): p. 525-538.
8. Kłoda, T., et al., *Strong-field photoionization of O 2 at intermediate light intensity.* Physical Review A, 2010. **82**(3): p. 033431.
9. Loh, Z.-H., et al., *Observation of the fastest chemical processes in the radiolysis of water.* Science, 2020. **367**(6474): p. 179-182.
10. Mourou, G.A., T. Tajima, and S.V. Bulanov, *Optics in the relativistic regime.* Reviews of modern physics, 2006. **78**(2): p. 309.
11. Marklund, M. and P.K. Shukla, *Nonlinear collective effects in photon-photon and photon-plasma interactions.* Reviews of modern physics, 2006. **78**(2): p. 591.
12. Fedotov, A., et al., *Advances in QED with intense background fields.* Physics Reports, 2023. **1010**: p. 1-138.
13. Protopapas, M., C.H. Keitel, and P.L. Knight, *Atomic physics with super-high intensity lasers.* Reports on Progress in Physics, 1997. **60**(4): p. 389.
14. Di Piazza, A., et al., *Extremely high-intensity laser interactions with fundamental quantum systems.* Reviews of Modern Physics, 2012. **84**(3): p. 1177.
15. Couairon, A. and A. Mysyrowicz, *Femtosecond filamentation in transparent media.* Physics reports, 2007. **441**(2-4): p. 47-189.
16. Trebino, R., *Frequency-Resolved Optical Gating: The Measurement of Ultrashort Laser Pulses*. 2000: Springer Science & Business Media.
17. Nagy, T., P. Simon, and L. Veisz, *High-energy few-cycle pulses: post-compression techniques.* Advances in Physics: X, 2021. **6**(1): p. 1845795.
18. Rolland, C. and P.B. Corkum, *Compression of high-power optical pulses.* JOSA B, 1988. **5**(3): p. 641-647.
19. Lu, C.-H., et al., *Generation of intense supercontinuum in condensed media.* Optica, 2014. **1**(6): p. 400-406.
20. Kaumanns, M., et al., *Multipass spectral broadening of 18 mJ pulses compressible from 1.3 ps to 41 fs.* Optics letters, 2018. **43**(23): p. 5877-5880.
21. Chen, X., et al., *Generation of 4.3 fs, 1 mJ laser pulses via compression of circularly polarized pulses in a gas-filled hollow-core fiber.* Optics letters, 2009. **34**(10): p. 1588-1590.
22. Boyd, R.W., *Nonlinear optics*. 2020: Academic press.
23. Dutin, C.F., et al., *Post-compression of high-energy femtosecond pulses using gas ionization.* Optics letters, 2010. **35**(2): p. 253-255.
24. Tempea, G. and T. Brabec, *Nonlinear source for the generation of high-energy few-cycle optical pulses.* Optics letters, 1998. **23**(16): p. 1286-1288.
25. Koprinkov, I., et al., *Self-compression of high-intensity femtosecond optical pulses and spatiotemporal soliton generation.* Physical review letters, 2000. **84**(17): p. 3847.
26. Wagner, N.L., et al., *Self-compression of ultrashort pulses through ionization-induced spatiotemporal reshaping.* Physical Review Letters, 2004. **93**(17): p. 173902.
27. Couairon, A., et al., *Pulse self-compression to the single-cycle limit by filamentation in a gas with a pressure gradient.* Optics letters, 2005. **30**(19): p. 2657-2659.
28. Stibenz, G., N. Zhavoronkov, and G. Steinmeyer, *Self-compression of millijoule pulses to 7.8 fs duration in a white-light filament.* Optics letters, 2006. **31**(2): p. 274-276.
29. Skupin, S., et al., *Self-compression by femtosecond pulse filamentation: Experiments versus numerical simulations.* Physical Review E, 2006. **74**(5): p. 056604.
30. Mysyrowicz, A., A. Couairon, and U. Keller, *Self-compression of optical laser pulses by filamentation.* New Journal of Physics, 2008. **10**(2): p. 025023.
31. Couairon, A., H.S. Chakraborty, and M.B. Gaarde, *From single-cycle self-compressed filaments to isolated attosecond pulses in noble gases.* Physical Review A, 2008. **77**(5): p. 053814.
32. Travers, J.C., et al., *High-energy pulse self-compression and ultraviolet generation through soliton dynamics in hollow capillary fibres.* Nature Photonics, 2019. **13**(8): p. 547-554.
33. Henz, S. and J. Herrmann, *Self-channeling and pulse shortening of femtosecond pulses in multiphoton-ionized dispersive dielectric solids.* Physical Review A, 1999. **59**(3): p. 2528.
34. Ward, H. and L. Bergé, *Temporal shaping of femtosecond solitary pulses in photoionized media.* Physical review letters, 2003. **90**(5): p. 053901.
35. Chen, X., et al., *Pulse self-compression in normally dispersive bulk media.* Optics communications, 2006. **259**(1): p. 331-335.
36. Ritus, A. and A. Manenkov, *Stimulated Mandel'shtam-Brillouin scattering in fused and crystalline quartz without damage to samples at T= 300° K.* Soviet Journal of Experimental and Theoretical Physics Letters, 1967. **6**: p. 349.
37. Chimier, B., et al., *Damage and ablation thresholds of fused-silica in femtosecond regime.* Physical Review B, 2011. **84**(9): p. 094104.
38. Hemmer, M., et al., *Self-compression to sub-3-cycle duration of mid-infrared optical pulses in dielectrics.* Optics express, 2013. **21**(23): p. 28095-28102.
39. Shumakova, V., et al., *Multi-millijoule few-cycle mid-infrared pulses through nonlinear self-compression in bulk.* Nature communications, 2016. **7**(1): p. 1-6.
40. He, Z.-H., et al., *Ionization-induced self-compression of tightly focused femtosecond laser pulses.* Physical review letters, 2014. **113**(26): p. 263904.
41. Xie, X., A.L. Cavalieri, and S.L. Johnson, *Self-compression of femtosecond laser pulses in ambient air through conical radiation.* Optics Letters, 2023. **48**(19): p. 5101-5104.
42. Mitrofanov, A., et al., *Self-compression of high-peak-power mid-infrared pulses in anomalously dispersive air.* optica, 2017. **4**(11): p. 1405-1408.

43. Hauri, C., et al., *Generation of intense, carrier-envelope phase-locked few-cycle laser pulses through filamentation.* Applied Physics B, 2004. **79**(6): p. 673-677.
44. Couairon*, A., et al., *Self-compression of ultra-short laser pulses down to one optical cycle by filamentation.* Journal of Modern Optics, 2006. **53**(1-2): p. 75-85.
45. Schulz, E., et al., *Intense few-cycle laser pulses from self-compression in a self-guiding filament.* Applied Physics B, 2009. **95**(2): p. 269-272.
46. Guandalini, A., et al., *5.1 fs pulses generated by filamentation and carrier envelope phase stability analysis.* Journal of Physics B: Atomic, Molecular and Optical Physics, 2006. **39**(13): p. S257.
47. Zaïr, A., et al., *Spatio-temporal characterization of few-cycle pulses obtained by filamentation.* Optics express, 2007. **15**(9): p. 5394-5405.
48. Kretschmar, M., et al., *Direct observation of pulse dynamics and self-compression along a femtosecond filament.* Optics express, 2014. **22**(19): p. 22905-22916.
49. Trisorio, A. and C. Hauri, *Control and characterization of multiple circularly polarized femtosecond filaments in argon.* Optics letters, 2007. **32**(12): p. 1650-1652.
50. Schimpf, D.N., et al., *Circular versus linear polarization in laser-amplifiers with Kerr-nonlinearity.* Optics express, 2009. **17**(21): p. 18774-18781.
51. Balciunas, T., et al., *A strong-field driver in the single-cycle regime based on self-compression in a kagome fibre.* Nature communications, 2015. **6**(1): p. 1-7.
52. Mollenauer, L.F., et al., *Extreme picosecond pulse narrowing by means of soliton effect in single-mode optical fibers.* Optics letters, 1983. **8**(5): p. 289-291.
53. Tai, K. and A. Tomita, *1100× optical fiber pulse compression using grating pair and soliton effect at 1.319 µm.* Applied physics letters, 1986. **48**(16): p. 1033-1035.
54. Gouveia-Neto, A., A. Gomes, and J. Taylor, *Generation of 33-fsec pulses at 1.32 µm through a high-order soliton effect in a single-mode optical fiber.* Optics letters, 1987. **12**(6): p. 395-397.
55. Agrawal, G.P., *Nonlinear fiber optics*, in *Nonlinear Science at the Dawn of the 21st Century*. 2000, Springer. p. 195-211.
56. Dianov, E., et al., *Optimal compression of multi-soliton pulses in optical fibers.* Sov. Tech. Phys. Lett, 1986. **12**(6): p. 311-313.
57. Chen, C.-M. and P.L. Kelley, *Nonlinear pulse compression in optical fibers: scaling laws and numerical analysis.* JOSA B, 2002. **19**(9): p. 1961-1967.
58. Travers, J.C., et al., *Ultrafast nonlinear optics in gas-filled hollow-core photonic crystal fibers.* JOSA B, 2011. **28**(12): p. A11-A26.
59. Mak, K., et al., *Two techniques for temporal pulse compression in gas-filled hollow-core kagomé photonic crystal fiber.* Optics letters, 2013. **38**(18): p. 3592-3595.
60. Debord, B., et al., *Multi-meter fiber-delivery and pulse self-compression of milli-Joule femtosecond laser and fiber-aided laser-micromachining.* Optics express, 2014. **22**(9): p. 10735-10746.
61. Gebhardt, M., et al., *Nonlinear pulse compression to 43 W GW-class few-cycle pulses at 2 µm wavelength.* Optics letters, 2017. **42**(20): p. 4179-4182.
62. Elu, U., et al., *High average power and single-cycle pulses from a mid-IR optical parametric chirped pulse amplifier.* Optica, 2017. **4**(9): p. 1024-1029.
63. Stepanov, E.A., et al., *Multioctave supercontinua from shock-coupled soliton self-compression.* Physical Review A, 2019. **99**(3): p. 033855.
64. Ermolov, A., et al., *Carrier-envelope-phase-stable soliton-based pulse compression to 4.4 fs and ultraviolet generation at the 800 kHz repetition rate.* Optics letters, 2019. **44**(20): p. 5005-5008.
65. Köttig, F., et al., *Efficient single-cycle pulse compression of an ytterbium fiber laser at 10 MHz repetition rate.* Optics Express, 2020. **28**(7): p. 9099-9110.
66. Savitsky, I., et al., *Sub-cycle pulse revealed with carrier-envelope phase control of soliton self-compression in anti-resonant hollow-core fiber.* Optics Letters, 2023. **48**(17): p. 4468-4471.
67. Anderson, P., et al., *High-energy laser-pulse self-compression in short gas-filled fibers.* Physical Review A, 2014. **89**(1): p. 013819.
68. Courtois, C., et al., *Propagation of intense ultrashort laser pulses in a plasma filled capillary tube: Simulations and experiments.* Physics of Plasmas, 2001. **8**(7): p. 3445-3456.
69. Skobelev, S.A., et al., *Ionization self-compression of intense femtosecond pulses propagating through gas-filled dielectric capillaries.* JETP letters, 2009. **89**(11): p. 540-546.
70. Brahms, C., F. Belli, and J.C. Travers, *Infrared attosecond field transients and UV to IR few-femtosecond pulses generated by high-energy soliton self-compression.* Physical Review Research, 2020. **2**(4): p. 043037.
71. Kelley, P., *Self-focusing of optical beams.* Physical Review Letters, 1965. **15**(26): p. 1005.
72. Gaeta, A.L., *Catastrophic collapse of ultrashort pulses.* Physical Review Letters, 2000. **84**(16): p. 3582.
73. Marcinkevičiūtė, A., et al., *A compact, self-compression-based sub-3 optical cycle source in the spectral range.* Journal of Optics, 2017. **19**(10): p. 105505.
74. Chen, X., et al., *Self-compression of loosely focused pulses in gases with power close to self-focusing critical value.* Chinese Optics Letters, 2007. **5**(101): p. S159-S162.
75. Hauri, C., et al., *Intense self-compressed, self-phase-stabilized few-cycle pulses at 2 µm from an optical filament.* Optics letters, 2007. **32**(7): p. 868-870.
76. Trunov, V., et al. *Spatiotemporal reshaping and compression of high intensity femtosecond pulses*. in *ICONO 2007: Nonlinear Space-Time Dynamics*. 2007. International Society for Optics and Photonics.
77. Akturk, S., et al., *Spectrogram representation of pulse self compression by filamentation.* Optics Express, 2008. **16**(22): p. 17626-17636.
78. Maurel, M., et al. *Soliton self-compression in air filled Kagome HCPCF*. in *2019 Conference on Lasers and Electro-Optics Europe & European Quantum Electronics Conference (CLEO/Europe-EQEC)*. 2019. IEEE.
79. Kurilova, M.V., et al., *Generation of optical pulses of duration down to 8 fs upon filamentation of collimated femtosecond laser radiation in argon.* Quantum Electronics, 2009. **39**(10): p. 879.
80. Gröbmeyer, S., et al., *Self-compression at 1 µm wavelength in all-bulk multi-pass geometry.* Applied Physics B, 2020. **126**(10): p. 1-6.
81. Mücke, O.D., et al., *Self-compression of millijoule 1.5 µm pulses.* Optics letters, 2009. **34**(16): p. 2498-2500.
82. Brahms, C., F. Belli, and J.C. Travers. *High-energy infrared soliton dynamics in hollow capillary fibres*. in *2020 Conference on Lasers and Electro-Optics (CLEO)*. 2020. IEEE.

83. Gao, Y., et al., *Generation of annular femtosecond few-cycle pulses by self-compression and spatial filtering in solid thin plates.* Optics Express, 2021. **29**(19): p. 29789-29801.
84. Otsuka, T., et al. *Propagation dynamics of an ultrashort, high energy laser pulse via self-modulation in gas medium with atmospheric pressure for laser compression*. in *Journal of Physics: Conference Series*. 2010. IOP Publishing.
85. Ran, Q., et al., *Self-compression of mJ pulses to 10 fs in a hollow-core waveguide: effects of higher-order dispersion.* JOSA B, 2022. **39**(3): p. A1-A8.
86. Varela, O., et al., *Self-compression controlled by the chirp of the input pulse.* Optics letters, 2010. **35**(21): p. 3649-3651.
87. Chernev, P. and V. Petrov, *Self-focusing of light pulses in the presence of normal group-velocity dispersion.* Optics letters, 1992. **17**(3): p. 172-174.
88. Fibich, G., V. Malkin, and G. Papanicolaou, *Beam self-focusing in the presence of a small normal time dispersion.* Physical Review A, 1995. **52**(5): p. 4218.
89. Ranka, J.K., R.W. Schirmer, and A.L. Gaeta, *Observation of pulse splitting in nonlinear dispersive media.* Physical Review Letters, 1996. **77**(18): p. 3783.
90. Fibich, G. and G. Papanicolaou, *Self-focusing in the perturbed and unperturbed nonlinear Schrödinger equation in critical dimension.* SIAM Journal on Applied Mathematics, 1999. **60**(1): p. 183-240.
91. Couairon, A., *Dynamics of femtosecond filamentation from saturation of self-focusing laser pulses.* Physical Review A, 2003. **68**(1): p. 015801.
92. LeMesurier, B.J., *Dissipation at singularities of the nonlinear Schrödinger equation through limits of regularisations.* Physica D: Nonlinear Phenomena, 2000. **138**(3-4): p. 334-343.
93. Zharova, N.A.e., A.G.e. Litvak, and V.A. Mironov, *On the collapse of wave packets in a medium with normal group velocity dispersion.* Journal of Experimental and Theoretical Physics Letters, 2002. **75**(11): p. 539-542.
94. Aközbek, N., et al., *White-light continuum generation and filamentation during the propagation of ultra-short laser pulses in air.* Optics communications, 2001. **191**(3-6): p. 353-362.
95. Kandidov, V., et al., *Self-transformation of a powerful femtosecond laser pulse into a white-light laser pulse in bulk optical media (or supercontinuum generation).* Applied Physics B, 2003. **77**(2): p. 149-165.
96. Dubietis, A., et al., *Ultrafast supercontinuum generation in bulk condensed media.* Lithuanian Journal of Physics, 2017. **57**(3).
97. Hauri, C., et al., *Generation of high-fidelity, down-chirped sub-10 fs mJ pulses through filamentation for driving relativistic laser-matter interactions at 1 kHz.* Applied physics letters, 2006. **89**(15): p. 151125.
98. Kim, A., et al., *Compression and frequency up-conversion of an ultrashort ionizing pulse in a plasma.* Physical Review A, 1990. **42**(4): p. 2493.
99. Bohman, S., et al., *Generation of 5.0 fs, 5.0 mJ pulses at 1kHz using hollow-fiber pulse compression.* Optics letters, 2010. **35**(11): p. 1887-1889.
100. Tournois, P., *Acousto-optic programmable dispersive filter for adaptive compensation of group delay time dispersion in laser systems.* Optics communications, 1997. **140**(4-6): p. 245-249.
101. Verluise, F., et al., *Amplitude and phase control of ultrashort pulses by use of an acousto-optic programmable dispersive filter: pulse compression and shaping.* Optics letters, 2000. **25**(8): p. 575-577.
102. Weiner, A.M., et al., *Programmable femtosecond pulse shaping by use of a multielement liquid-crystal phase modulator.* Optics letters, 1990. **15**(6): p. 326-328.
103. Weiner, A.M., et al., *Programmable shaping of femtosecond optical pulses by use of 128-element liquid crystal phase modulator.* IEEE journal of quantum electronics, 1992. **28**(4): p. 908-920.
104. Wefers, M.M. and K.A. Nelson, *Generation of high-fidelity programmable ultrafast optical waveforms.* Optics letters, 1995. **20**(9): p. 1047-1049.
105. Dugan, M., J. Tull, and W. Warren, *High-resolution acousto-optic shaping of unamplified and amplified femtosecond laser pulses.* JOSA B, 1997. **14**(9): p. 2348-2358.
106. Arbabi, A., et al., *Dielectric metasurfaces for complete control of phase and polarization with subwavelength spatial resolution and high transmission.* Nature nanotechnology, 2015. **10**(11): p. 937-943.
107. Divitt, S., et al., *Ultrafast optical pulse shaping using dielectric metasurfaces.* Science, 2019. **364**(6443): p. 890-894.
108. Safaei, R., et al., *High-energy multidimensional solitary states in hollow-core fibres.* Nature Photonics, 2020. **14**(12): p. 733-739.
109. Tian, Y., et al., *Tapered optical fiber sensor for label-free detection of biomolecules.* Sensors, 2011. **11**(4): p. 3780-3790.
110. Harun, S.W., et al., *Dual wavelength erbium-doped fiber laser using a tapered fiber.* Journal of Modern Optics, 2010. **57**(21): p. 2111-2113.
111. Giglio, M., et al., *Low-loss and single-mode tapered hollow-core waveguides optically coupled with interband and quantum cascade lasers.* Optical Engineering, 2017. **57**(1): p. 011004.
112. Gibson, D.J. and J.A. Harrington, *Gradually tapered hollow glass waveguides for the transmission of CO 2 laser radiation.* Applied optics, 2004. **43**(11): p. 2231-2235.
113. Matsuura, Y., et al., *Lensed-taper launching coupler for small-bore, infrared hollow fibers.* Applied optics, 1997. **36**(30): p. 7818-7821.
114. Ilev, I.K. and R.W. Waynant, *Grazing-incidence-based hollow taper for infrared laser-to-fiber coupling.* Applied physics letters, 1999. **74**(20): p. 2921-2923.
115. Narita, S., Y. Matsuura, and M. Miyagi, *Tapered hollow waveguide for focusing infrared laser beams.* Optics letters, 2007. **32**(8): p. 930-932.
116. Harun, S.W., et al., *Theoretical analysis and fabrication of tapered fiber.* Optik, 2013. **124**(6): p. 538-543.
117. Wan, Y. and W. Chang, *Effect of decreasing pressure on soliton self-compression in higher-order modes of a gas-filled capillary.* Optics Express, 2021. **29**(5): p. 7070-7083.
118. López-Zubieta, B.A., et al., *Theoretical analysis of single-cycle self-compression of near infrared pulses using high-spatial modes in capillary fibers.* Optics express, 2018. **26**(5): p. 6345-6350.